

Experimental Investigation of Fault-Tolerant Control Strategies for Quad-Inverter Converters

G. Grandi¹, P. Sanjeevikumar¹, Y. Gritli^{1,2}, F. Filippetti¹

¹Dept. of Electrical Engineering, University of Bologna, Bologna – Italy

²National Institute of Applied Sciences and Technology, University of Carthage, Tunis –Tunisia

Abstract– Fault-tolerant control strategies for quad-inverter based multiphase-multilevel converters are proposed and experimentally verified in this paper. Explicitly, the conversion scheme consists of four standard 2-level three-phase voltage source inverters (VSIs), able to supply a dual three-phase induction motor in open-end stator winding configuration (asymmetric six-phase machine), quadrupling the utility power of a single VSI within given voltage and current ratings. The developed modulation scheme has the capability to generate multilevel output voltage waveforms in healthy conditions, equivalent to the one of a 3-level VSI, and to share the total motor power among the four dc sources in each switching cycle. This sharing potentiality is investigated under post-fault operating conditions, when one VSI completely insulated due to a severe failure on it. In such circumstances, the quad-inverter system can perform with reduced power rating by a proper modulation of the remaining three healthy VSIs. The complete multiphase-multilevel conversion system with the proposed control algorithm under healthy and post-fault operating conditions has been verified by experimental implementation in open-loop control aspect using two dsp TMS320-F2812 processors with two three-phase passive loads in open-end configuration.

Index Terms– Multilevel inverter, multiphase inverter, post-fault-tolerance, space vector modulation, power balancing.

I. INTRODUCTION

Fault-tolerability in ac high power traction systems is a key item with high-voltage/high-current applications, where availability and reliability of performances are mandatory. More specifically, in this type of application, induction motors operate continuously in dynamic conditions, requiring frequent start/stop with rapid speed variations. Subsequently, the drives are regularly subjected to abuse of over-current surges and voltage over-swings. Recent research carried out on different failure possibilities in induction motor drives by industrials and experts have revealed that 21% are related to the stator windings and its configuration modularity [1]. Several phenomena can affect its reliability, such as mechanical and/or thermal stress, leading to severe failure modes such as inter-turn short-circuits, line-to-line, line-to-ground, multi-phase line-to-ground and multi-phase faults. A detailed analysis of these types of fault, its propagation modes and the appropriate diagnosis techniques can be found in [1]-[3].

Among various innovation and approaches in literatures relating to fault-tolerant performances, multi-phase ac machine technologies have been widely recognized as a viable solution [4]. More specifically, multi-phase drives are very advantageous in high power ac traction applications, thanks to its inherent active redundant structure, which improve considerably the system reliability. It takes only two phases (having independent currents) to create a fundamental m.m.f distribution rotating at the supply frequency, so a machine with m-phases can continue to operate at reduced power in a controlled manner, with $m-2$ open phases. Therefore, multi-phase inverters together with multi-phase ac machines have been proved as a fruitful solution, also providing high power ratings with current-

limited devices [4]-[5]. Other investigations to increase the power ratings have focused their efforts on multilevel inverters, being advantageous in terms of high voltages that can be provided using sources and switching devices with reduced voltage ratings. Additional benefits such as reduced harmonic distortion and lower dv/dt in the output voltages make this solution very suitable for industry applications [6]-[7]. Additional topologies, based on passive or/and active semiconductors, have been proposed for the same purposes, but the lower reliability still remain their major drawback [8]-[9]. A wide investigation of the reliability of inverter topologies has revealed that its estimated mean time between failures (MTBFs) is of about 2 years [10].

Among the proposed modern topologies, the conventional 2-level three-phase voltage source inverter still remains a mature technology. However, all types of inverters are still vulnerable to different potential anomalies, leading to an imminent total failure. Recent survey on inverters has revealed that (31-37.9)% of failures are caused by power parts [10] and the main failure mechanisms in modern power modules with IGBT devices for high-power applications can be found in [11]. Most potential sources of failures based on power devices, capacitors and gate control are detailed in [12]. Specifically, in both high power generation and traction systems, where availability is mandatory, once the fault is detected and localized, the ability to tolerate faults with safe operation is a key item in this type of applications. In this sense, innovative topologies based on a proper arrangement of conventional 2-level three-phase voltage source inverters (VSIs) to realize both multi-phase [13]-[14] and multilevel [15]-[18] inverters, have been investigated. The reduced cost of both inverter and motor due to conventional slot/winding configurations, and modularity of the whole conversion structure, with high reliability in power layout, are the main advantages of such topologies.

Motivated by the above considerations, and taking into account the low reliability of commercial inverters becoming more and more integrated, which reduce considerably its maintainability or reconfiguration [12], a novel structure based on a dual three-phase open-end winding motor (asymmetric six-phase induction machine) has been considered in this paper. The power supply consists of four standard 2-level three-phase VSIs having insulated dc sources to prevent circulation of zero-sequence current components and improving the reliability. The topology of the investigated structure, with its corresponding equivalent circuit in terms of three-phase space vectors, are reported by Fig. 1a and Fig. 1b respectively. It is important to note that the structure is easy scalable to nine, twelve or higher number of phases multiple of three. A modulation strategy has been utilized to regulate each couple of 2-level VSIs such as a 3-level, inverter given by [18], providing proper multilevel voltage waveforms for each three-phase stator winding. Furthermore, the proposed control algorithm allows total motor power to be shared among the four dc sources with three degrees of freedom [19]-[21].

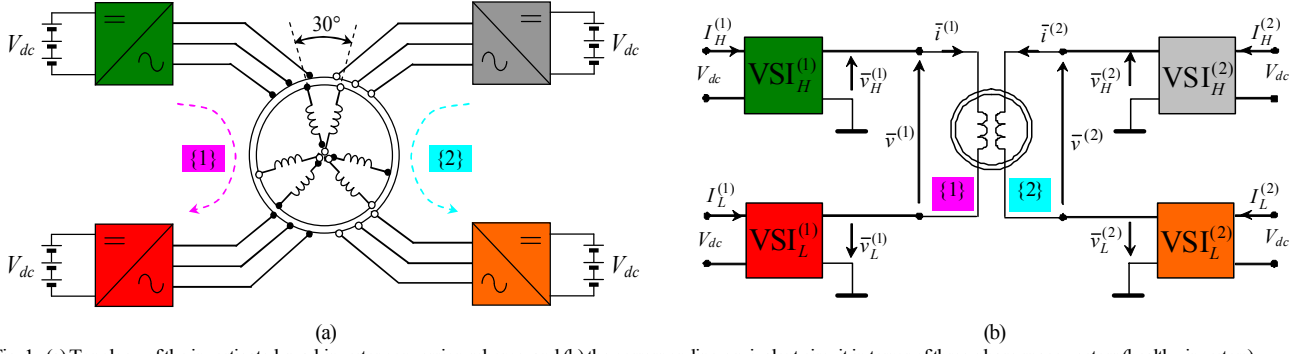


Fig. 1. (a) Topology of the investigated quad-inverter conversion scheme, and (b) the corresponding equivalent circuit in terms of three-phase space vectors (healthy inverters).

In perspective view, the proposed contribution is devoted to investigate inherent active redundancy of the used quad-inverter, under one, two or three failed inverters, to ensure system operability in the degraded modes given by [22]. In this paper, once the fault is diagnosed, the post-fault operating condition under one severe failed inverter is investigated by experimental tests, to confirm the simulation results given in [23]. The resulting two degrees of freedom are exploited, if/when required, either to balance power sharing between the two three-phase motor windings (with minimization of power losses), or to balance the power sharing among the three remaining dc sources.

II. BASICS OF THE QUAD-INVERTER CONVERSION SCHEME

Multiple space vectors are considered to represent the variables of the whole six-phase system consisting of the dual three-phase machine supplied by four three-phase VSIs with insulated dc supplies. In particular, the asymmetric six-phase space vector transformations introduced in [13], [14] are considered.

In the case of a dual three-phase induction motor having sinusoidal distributed stator windings, the machine behavior can be described in terms of multiple space vectors by the following equations, in a stationary reference frame [14]:

$$\bar{v}_{S1} = R_S \bar{i}_{S1} + \frac{d\bar{\varphi}_{S1}}{dt}, \bar{\varphi}_{S1} = L_{S1} \bar{i}_{S1} + M_1 \bar{i}_{R1}, \quad (1)$$

$$0 = R_R \bar{i}_{R1} - j p \omega_m \bar{\varphi}_{R1} + \frac{d\bar{\varphi}_{R1}}{dt}, \bar{\varphi}_{R1} = M_1 \bar{i}_{S1} + L_{R1} \bar{i}_{R1}, \quad (2)$$

$$\bar{v}_{S5} = R_S \bar{i}_{S5} + \frac{d\bar{\varphi}_{S5}}{dt}, \bar{\varphi}_{S5} = L_{S5} \bar{i}_{S5}, \quad (3)$$

$$T = 3p M_1 \bar{i}_{S1} \cdot j \bar{i}_{R1}, \quad (4)$$

where p is the pole pairs number, ω_m is the rotor angular speed, and the subscripts S and R denote stator and rotor quantities, respectively. It should be noted that the sinusoidal spatial distribution of the magnetic field in the air gap is mainly generated by the space vectors \bar{i}_{S1} and \bar{i}_{R1} , whereas \bar{i}_{S5} does not contribute to the air gap field.

The total motor power P can be expressed by [21]:

$$P = P^{(1)} + P^{(2)} = \frac{3}{2} \left[(\bar{v}_H^{(1)} + \bar{v}_L^{(1)}) \cdot \bar{i}^{(1)} + (\bar{v}_H^{(2)} + \bar{v}_L^{(2)}) \cdot \bar{i}^{(2)} \right], \quad (5)$$

being $P^{(1)}$ and $P^{(2)}$ the individual powers of the two three-phase stator windings {1} and {2} given by:

$$\begin{cases} P^{(1)} = \frac{3}{2} \bar{v}^{(1)} \cdot \bar{i}^{(1)} \\ P^{(2)} = \frac{3}{2} \bar{v}^{(2)} \cdot \bar{i}^{(2)} \end{cases}, \quad (6)$$

and the stator winding voltages $v^{(1)}$ and $v^{(2)}$ can be written as the sum of voltages of the individual inverters ‘‘H’’ and ‘‘L’’ as:

$$\begin{cases} \bar{v}^{(1)} = \bar{v}_H^{(1)} + \bar{v}_L^{(1)} \\ \bar{v}^{(2)} = \bar{v}_H^{(2)} + \bar{v}_L^{(2)} \end{cases}. \quad (7)$$

The total power can be shared among the four dc sources of the quad-inverter system with three-degrees of freedom, expressed by the three coefficients k_i , $k_v^{(1)}$, and $k_v^{(2)}$ [21].

The first coefficient k_i concerns with current and power sharing between the two three-phase windings {1} and {2}:

$$\begin{cases} \bar{i}^{(1)} = 2k_i \bar{i}_{S1} \\ \bar{i}^{(2)} = 2\alpha^{-1} (1 - k_i) \bar{i}_{S1} \end{cases}, \quad (8)$$

$$\begin{cases} P^{(1)} = P_H^{(1)} + P_L^{(1)} \cong k_i P \\ P^{(2)} = P_H^{(2)} + P_L^{(2)} \cong (1 - k_i) P \end{cases}. \quad (9)$$

The second $k_v^{(1)}$ and third $k_v^{(2)}$ coefficients are related to the voltage and power sharing between the two inverters ‘‘H’’ and ‘‘L’’ which supply each three-phase winding:

$$\begin{cases} \bar{v}_H^{(1)} = k_v^{(1)} \bar{v}^{(1)} \\ \bar{v}_L^{(1)} = (1 - k_v^{(1)}) \bar{v}^{(1)} \end{cases} \quad \begin{cases} \bar{v}_H^{(2)} = k_v^{(2)} \bar{v}^{(2)} \\ \bar{v}_L^{(2)} = (1 - k_v^{(2)}) \bar{v}^{(2)} \end{cases}, \quad (10)$$

$$\begin{cases} P_H^{(1)} = k_v^{(1)} P^{(1)} \\ P_L^{(1)} = (1 - k_v^{(1)}) P^{(1)} \end{cases} \quad \begin{cases} P_H^{(2)} = k_v^{(2)} P^{(2)} \\ P_L^{(2)} = (1 - k_v^{(2)}) P^{(2)} \end{cases}. \quad (11)$$

Note that, to equally share the motor power among the four inverters, i.e., 25% of the total power for each dc source, all sharing coefficients k_i , $k_v^{(1)}$, and $k_v^{(2)}$ must be set to 1/2.

In order to synthesize the voltage vectors $v^{(1)}$ and $v^{(2)}$, a proper multilevel SVM algorithm must be applied to satisfy also the power sharing between the two windings [18]. With reference to Fig. 2a, due to the symmetry of the outer hexagon, the analysis can be restricted to one of its six sectors (i.e., OAB), similarly to the case of conventional three-phase SVM algorithm. Furthermore, the main triangle OAB is divided in four identical equilateral triangles. The reference of voltage $v^{(1)}$ lays in one of these triangles, leading to four relevant cases. By the basic SVM principle, the components $v_H^{(1)}$ and $v_L^{(1)}$ can be generated by selecting adjacent

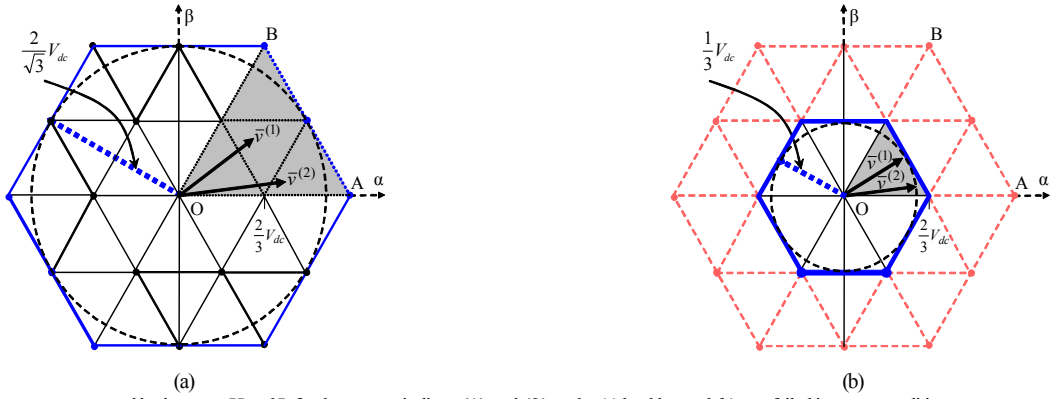


Fig. 2. Voltage space vectors generated by inverters H and L for the stator windings {1} and {2} under (a) healthy, and (b) one failed inverter conditions.

vectors. The switch configurations corresponding to these vectors cannot be applied in an arbitrary sequence if proper multilevel voltage waveforms are desired, i.e., the voltage $v^{(1)}$ should be generated by using the nearest three vectors approach (NTV) [21]. For this purpose, the method introduced in [18] has been implemented. The same considerations are valuable for the voltage $v^{(2)}$.

III. THE PROPOSED POST-FAULT-TOLERANT STRATEGIES

Integrated cooling technologies are widely employed in commercial inverter applications for high power ac traction system. Advantages of such technologies are ease-of-use, miniaturization and compactness in traction systems. However, the non-maintainability due to the compact packaging and the reduced thermal dissipation justifies the reduced reliability of the inverters [8], [11], [12].

Independently to the technology adopted, the inverters are still mainly subjected to several failures due to:

- dc-link electrolytic capacitor,
- dc bus voltage sensor,
- power semiconductor (either short- or open-circuit),
- control and driver circuits,

commonly known by their rapid propagation, leading to severe degrees of damage for the whole system.

For these reasons, once the fault is detected and localized in one among the four inverters, most of the times the concerned inverter can be considered as totally damaged and must be completely isolated. The failed inverter should be disconnected from both the motor and the dc source (battery), e.g. using bypass switches. Then, the developed control system is adapted in a manner that the ac motor drive machine still continues to operate in post-fault conditions.

Under the considered post-fault configuration, the pro-

posed control strategy allows continuity of operation, but with a reduced power range and loosing one degree of freedom in the power sharing among the dc sources: from three degrees, under healthy conditions, to two degrees.

In fact, supposing the fault occurs on inverter $VSI_L^{(1)}$, as represented in the equivalent circuit of Fig. 3, the corresponding dc source must be insulated, and the three output phases must be short-circuited to allow current circulation on stator winding {1}. The open-end winding configuration of the motor now collapse to traditional three-phase star connection in stator winding {1}, and the entire voltage for stator winding {1}, $\bar{v}^{(1)}$, must be provided by inverter $VSI_H^{(1)}$. About the voltage for stator winding {2}, $\bar{v}^{(2)}$, it can still be provided by both inverters $VSI_H^{(2)}$ and $VSI_L^{(2)}$.

Then, according to (10), the post-fault operating conditions can be summarized as:

$$\begin{cases} \bar{v}_L^{(1)} = 0 \\ \bar{v}_H^{(1)} = \bar{v}^{(1)} \end{cases} \iff k_v^{(1)} = 1. \quad (12)$$

Taking into account (9), (11), and (12), the individual inverter powers are now be expressed as:

$$\begin{cases} P_L^{(1)} = 0 \\ P_H^{(1)} \equiv k_i P \end{cases} \quad \begin{cases} P_L^{(2)} \equiv (1-k_i)(1-k_v^{(2)})P \\ P_H^{(2)} \equiv (1-k_i)k_v^{(2)}P \end{cases}. \quad (13)$$

Being $k_v^{(1)}$ imposed by the fault, the remaining two degree of freedoms are now represented by $k_v^{(2)}$ (i.e. voltage sharing between healthy inverters $VSI_H^{(2)}$ and $VSI_L^{(2)}$) and k_i (i.e. current sharing between the two three-phase winding {1} and {2}). In this paper, condition (12) will be applied in experimental tests to represent the post-fault conditions instead of using additional

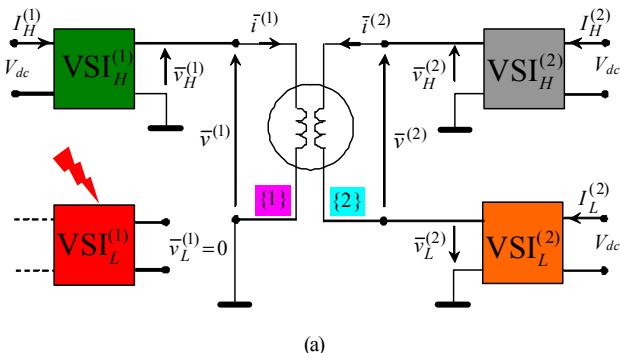


Fig. 3. Equivalent circuit of the post-fault configuration, in terms of three-phase space vectors, with one failed inverter, $v_L^{(1)}=0$.

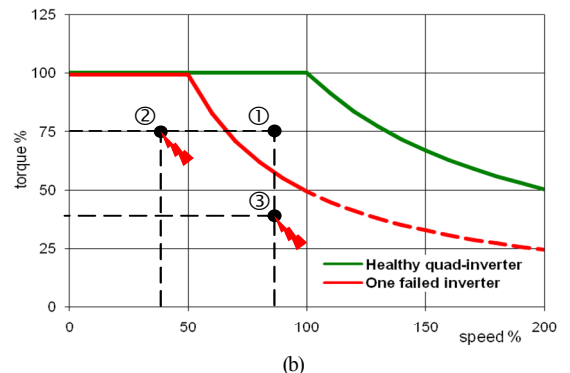


Fig. 4. Operating points under test in the torque versus speed diagram for healthy (4 VSIs) and one failed inverter (3 VSIs) conditions.

bypass switches for creating star connection on the faulty inverter and complete insulation and for current circulation. The first relevant consequence of the fault in one inverter is that the maximum output voltage for one of the two three-phase stator windings is halved. Then, since the two stator windings share the same magnetic circuit and have the same induced e.m.f., the maximum voltage of the other stator winding is halved as well, from $2/\sqrt{3}V_{dc}$ to $1/\sqrt{3}V_{dc}$, as emphasized in Fig. 2b, leading to a 50% reduction of the whole maximum motor power. The different working conditions are summarized in Fig. 4, with reference to the torque versus speed characteristics in healthy (green line) and faulty (red line) operating conditions.

As an example, the operating point ① can be implemented only in healthy conditions, whereas the operating points ② and ③ can be implemented also in post-fault conditions (the last one with a flux weakening to reduce the required stator winding voltage).

Different strategies can be introduced to realize the post-fault operating conditions, with the remaining three healthy VSIs. In this paper will be considered the two relevant cases of minimization of power losses and symmetrical power sharing among the three healthy VSIs (i.e., among the corresponding three dc sources).

A. Balanced power sharing between the two three-phase stator motor windings and minimization of power losses

As known, a balanced current sharing between the two three-phase windings leads to minimum stator copper losses. This can be simply implemented in post-fault conditions by setting $k_i = 1/2$, with arbitrary voltage sharing coefficient $k_v^{(2)}$ to synthesize $v^{(2)}$. Although the usage of both $VSI_H^{(2)}$ and $VSI_L^{(2)}$ allows an active redundancy, it is not optimal from the point of view of the inverter losses, involving two inverters when the desired output voltage could be synthesized with just one of them.

For this reason, the provision of a passive redundancy with one inverter for the winding {2} still considerably improve the reliability of the post-fault configuration but it reduces the whole converter losses. In this case, inverter $VSI_H^{(1)}$ can operate just with inverter $VSI_H^{(2)}$, whereas the output voltage of inverter $VSI_L^{(2)}$ can be set to zero, or vice versa, leading to exactly the same operating performances of the motor. The open-end windings configuration of the motor now collapse to traditional three-phase star connections for both stator windings. Voltage and power equations, (10), (9) and (11), in addition to the fault condition (12), can now be summarized as:

$$\begin{cases} \bar{v}_L^{(2)} = 0 \\ \bar{v}_H^{(2)} = \bar{v}^{(2)} \end{cases} \longleftrightarrow k_v^{(2)} = 1, \quad (14)$$

$$\begin{cases} P_L^{(1)} = 0 \\ P_H^{(1)} = \frac{1}{2}P \end{cases} \longleftrightarrow \begin{cases} P_L^{(2)} = 0 \\ P_H^{(2)} = \frac{1}{2}P \end{cases} \longleftrightarrow k_i = \frac{1}{2}. \quad (15)$$

B. Balanced power sharing among the three healthy VSIs

As a further step in this post-fault investigation, the point of interest is now to share the total motor power symmetrically among the three healthy inverters, i.e., among the three remaining dc sources. This behavior is recommended

for battery supplied traction systems, in which the balanced charge status of batteries can be considered as a crucial issue. In order to implement a balanced power sharing among the three dc power supplies, an unbalanced power sharing between the two three-phase windings {1} and {2} must be introduced. In particular, one third of the total motor power must be supplied by each VSI. According to (9)-(13), the following voltage and power equations can be written:

$$\begin{cases} \bar{v}_L^{(2)} = \frac{1}{2}\bar{v}^{(2)} \\ \bar{v}_H^{(2)} = \frac{1}{2}\bar{v}^{(2)} \end{cases} \longleftrightarrow k_v^{(2)} = \frac{1}{2}, \quad (16)$$

$$\begin{cases} P_L^{(1)} = 0 \\ P_H^{(1)} = \frac{1}{3}P \end{cases} \longleftrightarrow \begin{cases} P_L^{(2)} = \frac{1}{3}P \\ P_H^{(2)} = \frac{1}{3}P \end{cases} \longleftrightarrow k_i = \frac{1}{3}. \quad (17)$$

In the next section, simplified experimental tests under healthy and post-fault operating conditions are presented and discussed with reference both balanced and unbalanced power sharing approaches.

IV. EXPERIMENTAL RESULTS

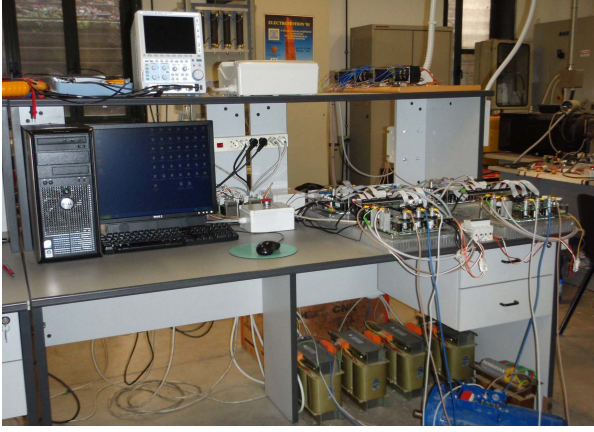
For the sake of simplicity, experimental tests are carried out by using a system of six RL impedance load in open-ends configuration instead of the dual three-phase induction motor. The main parameters of the four 2-level VSIs and six-phase load are given in Table I. Inverters are controlled in open-loop scheme using inverse three-phase space vector decomposition approach [21] with level-shifted pulse width modulation technique [24] for multilevel output phase voltages, and a phase shift of 30° is set as the displacement between the output voltages of the two dual three-phase inverters {1} and {2}.

The system consists in two processor boards, including a TMS320F2812 DSP each. The DSP-1 board acts as main control unit, performing all the calculations and providing for the firing signals of inverters H⁽¹⁾ and L⁽¹⁾ by its own internal PWM unit. The DSP-2 board acts as auxiliary unit, receiving the modulating signals from the DSP-1 by the multi-channel buffered serial port (McBSP data cable connection). DSP-2 provides for the firing signals of inverters H⁽²⁾ and L⁽²⁾ by its own internal PWM unit and individual modulation indices of four inverters, McBSP communication and PWM synchronization details are provided with preliminary experimental results in [25].

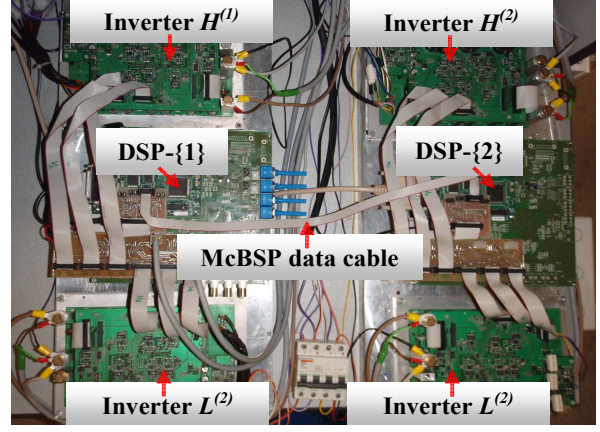
A picture of the working area in the Lab is given in Fig. 5a, whereas a detail view of control and power boards of the whole quad-inverter system is given in Fig. 5b.

TABLE I
MAIN PARAMETERS OF FOUR INVERTERS AND SIX-PHASE LOAD

	Vishay Siliconix SUM85N15-19
MOSFETs (6 in parallel per switch)	V _{DSS} =150 [V]; R _{DS(on)} =19[mΩ]@V _{GS} =10[V]; I _D =85[A]
MOSFET ratings	
switching frequency	2 [kHz]
dc-bus capacitance (4 banks)	12 [mF]
dc-bus voltage (4 in all)	52 [V]
load impedance (open ends, 6 in all)	6 [Ω]
load power factor (angle)	0.67 (48°)
load rated current	10 [A]



(a)



(b)

Fig. 5. Pictures of the experimental setup: (a) working area in Lab and (b) overall view of control and power boards of the quad-inverter system.

A. System performance in healthy condition

The healthy quad-inverter system is tested in balanced power condition with an open-loop scheme and a fundamental frequency of 50Hz, as represented by the operating point ① in Fig. 4. In this case, modulation indexes of the two dual-inverter {1} and {2} are $m^{(1)} = m^{(2)} = 0.9$, and individual modulation indexes of four VSIs are $m_H^{(1)} = m_L^{(1)} = m_H^{(2)} = m_L^{(2)} = 0.9$. In this way all sharing coefficients are set to $\frac{1}{2}$, as depicted in Fig. 6, and the total electrical power is equally shared among the four healthy VSIs.

Fig. 7 shows the open-winding voltages of the first-phase along with their time scaled average values, from top-to-bottom, $v_1^{(1)}$ (purple trace) and $v_1^{(2)}$ (turquoise trace) respectively. As expected, multilevel stepped waveforms appear with 9 levels, being the modulation index greater than 50% (outer hexagon shown in Fig. 2a) and the phase shift of 30° is noticed between the two winding voltages.

Fig. 8 shows, the six-phase currents of open-winding {1} ($i_1^{(1)}, i_2^{(1)}, i_3^{(1)}; i_{123}^{(1)}$, purple traces) and open-winding {2} ($i_1^{(2)}, i_2^{(2)}, i_3^{(2)}; i_{123}^{(2)}$, turquoise traces), respectively. It is observed that currents are almost sinusoidal, proving the effectiveness of the modulation strategy in healthy state when the total power is equally shared among the four VSIs.

B. System performance in post-fault conditions with one failed inverter

The following two experimental tests depicted in Figs. 9-11 and Figs. 12-14 are carried out for quad-inverter system with a fundamental frequency of 25Hz to represent the operating point ② shown in Fig. 4.

In the first time interval [0-30 ms] the quad-inverter operates in healthy balanced conditions with modulation indexes of the two dual-inverters $m^{(1)} = m^{(2)} = 0.32$, and individual modulation indexes of the four VSIs $m_H^{(1)} = m_L^{(1)} = m_H^{(2)} = m_L^{(2)} = 0.32$.

1) Balanced power sharing between the two three-phase open-end loads

Both the fault and the post-fault operating conditions are realized in hardware testing by exploiting the degrees of freedom without any additional by-pass switches or/ nor protective circuitry.

The variation of voltage and current sharing coefficients are shown by Fig. 9. As the fault occurs, at $t = 30$ ms, $k_v^{(1)}$ turns to 1. The post-fault strategy is applied at $t = 60$ ms, when $k_v^{(2)}$ turned to 1. The current sharing coefficient k_i remains unchanged in the entire time interval [0-90 ms].

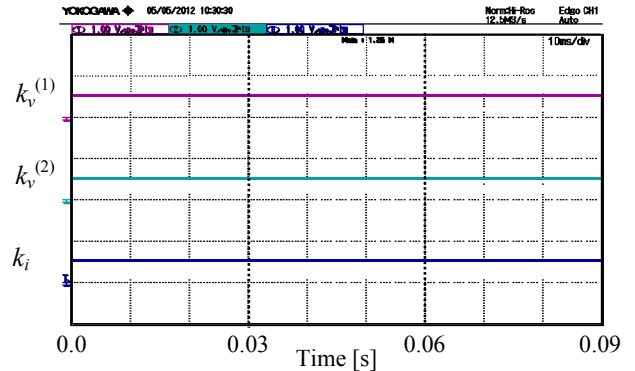


Fig. 6. Voltage and current sharing coefficients [1 unit/div].

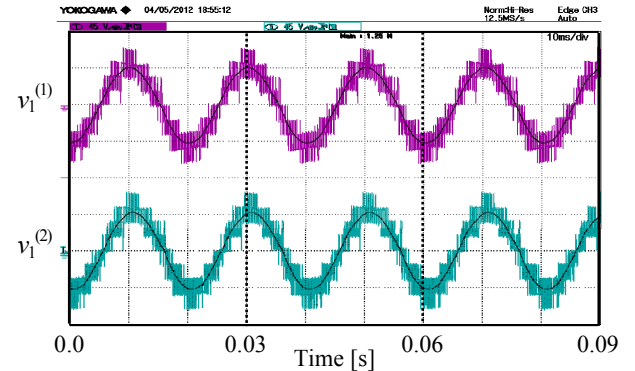


Fig. 7. First phases stator voltage with time scaled average components [45 V/div]. From top-to-bottom: winding {1} (purple trace); winding {2} (turquoise trace).

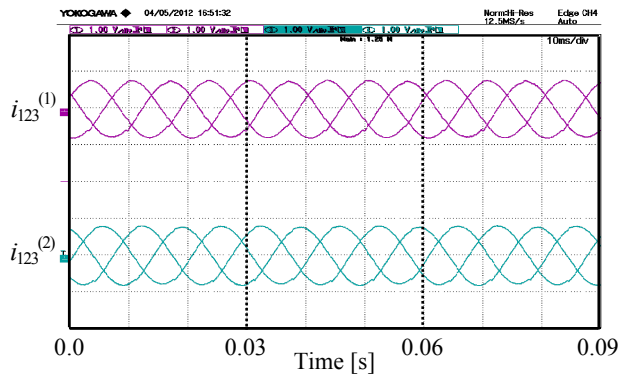


Fig. 8. Stator phase currents on windings {1} (purple trace) and {2} (turquoise trace). [10 A/div].

Fig. 10 shows, from top-to-bottom, the waveforms of artificial line-to-neutral voltages of 1st phase, $v_{H1}^{(1)}$, $v_{L1}^{(1)}$, $v_{H1}^{(2)}$, and $v_{L1}^{(2)}$ (green, red, gray, and orange traces, respectively). The averaged voltage values (i.e. fundamentals) are

also depicted on the corresponding diagrams. It is observed a 180° phase displacement between the two voltages on the same winding, and a 30° phase displacement between the voltages on different windings.

To be noticed, during first interval [0-30 ms], artificial line-to-neutral voltages of inverters (H and L) have the same amplitude, proving the effectiveness of the modulation strategy in balanced, healthy operating conditions.

At time $t = 30$ ms, when the fault occurs on inverter $VSI_L^{(1)}$, the corresponding voltage $v_{L1}^{(1)}$ (red trace) goes to zero, whereas the voltage on the other side of winding {1}, $VSI_H^{(1)}$, doubles its value $v_{H1}^{(1)}$ (green trace) to provide for the missing winding voltage, whereas voltages $VSI_H^{(2)}$ ($v_{H1}^{(2)}$, gray trace) and $VSI_L^{(2)}$ ($v_{L1}^{(2)}$, orange trace) are unaffected by the fault, being applied to the winding {2}, as confirmed by their respective fundamental component. In this faulty condition [30-60 ms] the modulation index of dual-inverter {1} and {2} are $m^{(1)} = m^{(2)} = 0.32$, and individual modulation indexes of inverters are $m_H^{(1)} = 0.64$, $m_L^{(1)} = 0$, $m_H^{(2)} = m_L^{(2)} = 0.32$.

As the first proposed post-fault strategy is applied, at $t = 60$ ms, $VSI_L^{(2)}$ is turned off by setting to zero the corresponding modulation index, $m_L^{(2)} = 0$, and the voltage of $VSI_H^{(2)}$ doubles its value to provide for the missing voltage on winding {2}. The remaining two active inverters $VSI_H^{(1)}$ and $VSI_H^{(2)}$ provide now the voltages with same amplitudes. To summarize this first post-fault condition, the modulation indexes of dual-inverters {1} and {2} are $m^{(1)} = m^{(2)} = 0.32$ and individual modulation indexes of the four VSIs are $m_H^{(1)} = m_H^{(2)} = 0.62$, $m_L^{(1)} = m_L^{(2)} = 0$.

Fig. 11 shows, the open-ends voltages of the first-phase along with their time scaled average values, from top-to-bottom, $v_1^{(1)}$ (purple trace) and $v_1^{(2)}$ (turquoise trace) respectively. As expected, phase voltages are unaffected either by the fault occurrence or by the application of post-fault control strategy. Now the multilevel stepped voltage waveforms appear with 5 levels, as for traditional 2-level inverters, being the modulation index lower than 50% (inner hexagon shown in Fig. 2b) during both healthy and faulty conditions.

The six-phase currents are shown in Fig. 12, for open-ends load {1} ($i_1^{(1)}$, $i_2^{(1)}$, $i_3^{(1)}$: $i_{123}^{(1)}$, purple traces) and open-ends load {2} ($i_1^{(2)}$, $i_2^{(2)}$, $i_3^{(2)}$: $i_{123}^{(2)}$, turquoise traces), respectively. Currents are almost sinusoidal and approximately 30° angle displaced. To be noticed that, as for phase voltages, currents are unaffected by fault and post-fault strategy occurrences, experimentally proving the effectiveness of the modulation strategy in healthy state (balanced power operation), faulty condition, and first post-fault control strategy with two operating VSIs ($VSI_H^{(1)}$ and $VSI_H^{(2)}$).

2) Balanced power sharing among the three healthy VSIs

The variation of voltage and current sharing coefficients are shown by Fig. 13. As the fault occurs, at $t = 30$ ms, $k_v^{(1)}$ turns to 1. The post-fault strategy is applied at $t = 60$ ms, when k_i is turned from 1/2 to 1/3. The voltage sharing coefficient $k_v^{(2)}$ remains unchanged in the entire time interval [0-90 ms].

Fig. 14 shows, from top-to-bottom, the waveforms of artificial line-to-neutral voltages of 1st phase, $v_{H1}^{(1)}$, $v_{L1}^{(1)}$, $v_{H1}^{(2)}$, and $v_{L1}^{(2)}$ (green, red, gray, and orange traces, respectively). The averaged voltage values (i.e. fundamentals) are also depicted on the corresponding diagrams. Again, it is

observed a 180° phase displacement between the two voltages on the same winding, and a 30° phase displacement between the voltages on different windings.

As in previous case, when the fault occurs on inverter $VSI_L^{(1)}$ at time $t = 30$ ms, the corresponding voltage $v_{L1}^{(1)}$ (red trace) goes to zero, whereas the voltage on the other side of winding {1}, $VSI_H^{(1)}$, doubles its value $v_{H1}^{(1)}$ (green trace) to provide for the missing winding voltage, whereas voltages $VSI_H^{(2)}$ ($v_{H1}^{(2)}$, gray trace) and $VSI_L^{(2)}$ ($v_{L1}^{(2)}$, orange trace) are unaffected by the fault, being applied to the winding {2}, as confirmed by their respective fundamental component. In this faulty condition [30-60 ms] the modulation index of dual-inverter {1} and {2} are $m^{(1)} = m^{(2)} = 0.32$, and individual modulation indexes of inverters are $m_H^{(1)} = 0.64$, $m_L^{(1)} = 0$, $m_H^{(2)} = m_L^{(2)} = 0.32$.

As the second proposed post-fault strategy is applied, at $t = 60$ ms, active inverters $VSI_H^{(1)}$, $VSI_H^{(2)}$ and $VSI_L^{(2)}$ provide now the voltages with same amplitudes, as remarked by their respective fundamental components.

To summarize this second post-fault condition, the modulation indexes of dual-inverters {1} and {2} are $m^{(1)} = 0.16$ and $m^{(2)} = 0.32$, respectively, and individual modulation indexes of the four VSIs are $m_H^{(1)} = m_H^{(2)} = m_L^{(2)} = 0.32$, and $m_L^{(1)} = 0$.

Fig. 15 shows, the open-ends voltages of the first-phase along with their time scaled average values, from top-to-bottom, $v_1^{(1)}$ (purple trace) and $v_1^{(2)}$ (turquoise trace) respectively. Again, as expected, phase voltages are unaffected either by the fault occurrence or by the application of post-fault control strategy. Also in this case, multilevel stepped voltage waveforms appear with 5 levels, as for traditional 2-level inverters, being the modulation index lower than 50% (inner hexagon shown in Fig. 2b) during both healthy and faulty conditions.

The six-phase winding currents are shown in the Fig. 16, for open-ends load {1} ($i_1^{(1)}$, $i_2^{(1)}$, $i_3^{(1)}$: $i_{123}^{(1)}$, purple traces) and open-ends load {2} ($i_1^{(2)}$, $i_2^{(2)}$, $i_3^{(2)}$: $i_{123}^{(2)}$, turquoise traces), respectively. Current are almost sinusoidal and approximately 30° angle displaced. The change of current sharing coefficient k_i from 1/2 to 1/3 leads to an increase of currents on load {2}, and to a decrease of currents on load {1}, becoming ones double of the others, according to (8).

The experimental test proves the effectiveness also of this second proposed post-fault modulation strategy with three power-balanced operating VSIs ($VSI_H^{(1)}$, $VSI_H^{(2)}$, and $VSI_L^{(2)}$).

V. CONCLUSIONS

A new quad-inverter multiphase-multilevel conversion topology was proposed and experimentally investigated in this paper in case of severe failures. The quad-inverter scheme is able to generate multilevel voltage waveforms during healthy state, equivalent to the ones of a 3-level inverter, and the developed modulation strategy is able to share the total load power among the four dc sources within each switching cycle, with three degree of freedom.

It has been verified that during post-fault conditions, with one failed inverter, the total power rating is reduced to the half, and one degree of freedom in the power sharing is lost. Significantly, the remaining two degrees of freedom can be exploited to equally share the total power between the two three-phase open-winding loads, leading to optimum inverter efficiency (also when suitably connected with

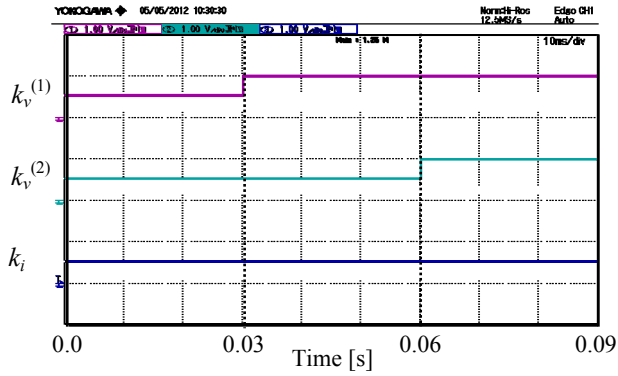


Fig. 9. Voltage and current sharing coefficients [1 unit/div].

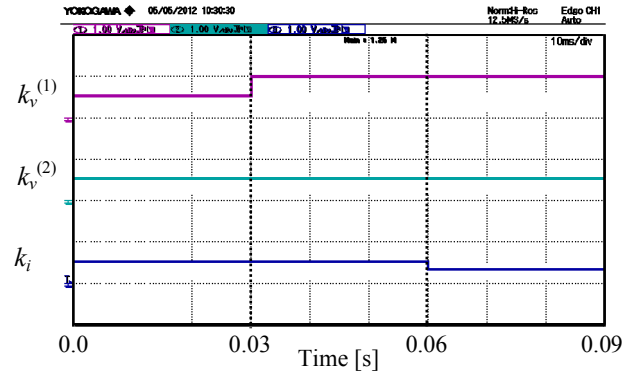


Fig. 13. Voltage and current sharing coefficients [1 unit/div].

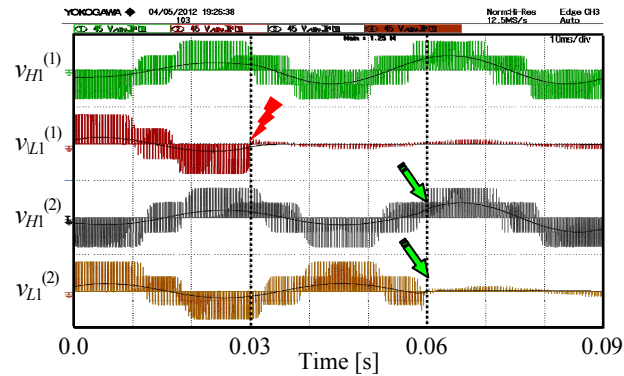


Fig. 10. Artificial line-to-neutral voltage (first phases) with their time scaled average components [45 V/div]. From top-to-bottom: dual-inverter {1}: H (green) and L (red) traces, dual-inverter {2}: H (gray) and L (orange) traces.

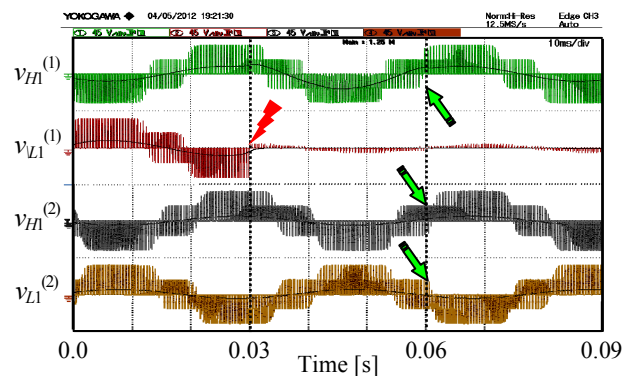


Fig. 14. Artificial line-to-neutral voltage (first phases) with their time scaled average components [45 V/div]. From top-to-bottom: dual-inverter {1}: H (green) and L (red) traces, dual-inverter {2}: H (gray) and L (orange) traces.

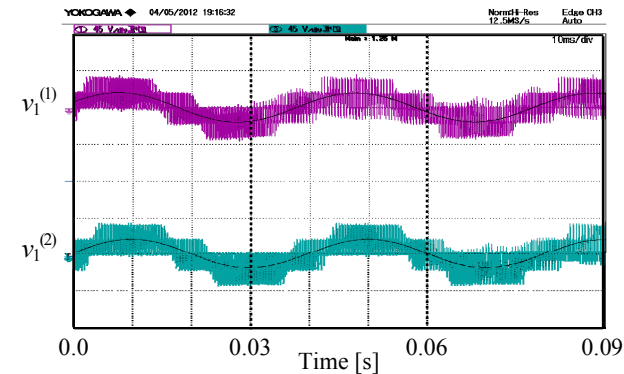


Fig. 11. First phases stator voltage with time scaled average components [45 V/div]. From top-to-bottom: winding {1} (purple trace); winding {2} (turquoise trace).

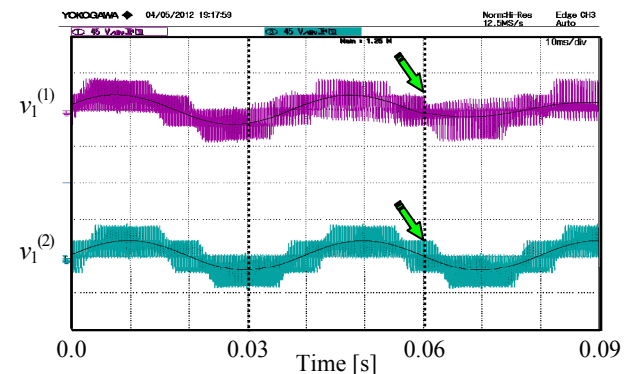


Fig. 15. First phases stator voltage with time scaled average components [45 V/div]. From top-to-bottom: winding {1} (purple trace); winding {2} (turquoise trace).

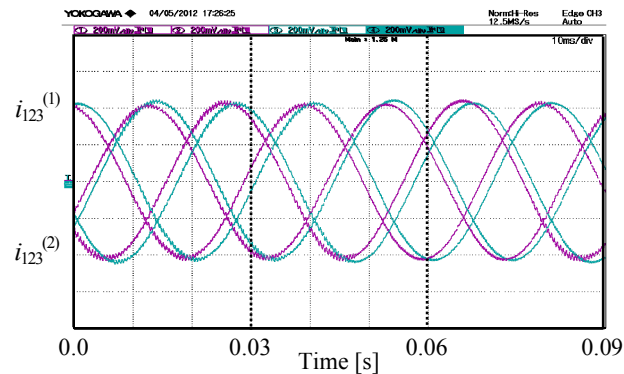


Fig. 12. Stator phase currents on windings {1} (purple trace) and {2} (turquoise trace). [2 A/div].

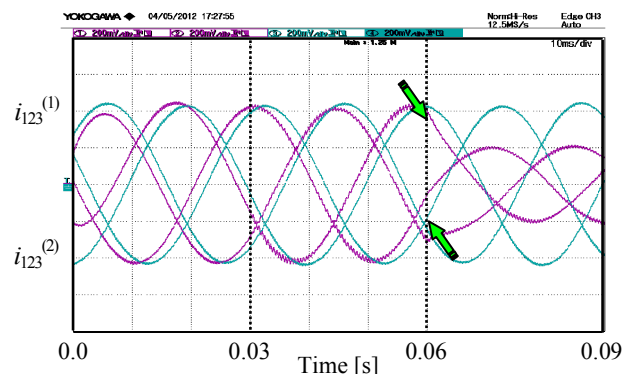


Fig. 16. Stator phase currents on windings {1} (purple trace) and {2} (turquoise trace). [2 A/div].

motor), or among the three remaining dc sources, leading to a balanced charge status in case of battery power supplies.

The hardware implementation has been carried out by using two DSP TMS320F2812 boards, each one controlling in open-loop mode a dual three-phase inverter, with a six-phase open-ends passive load.

Experimental tests show a good agreement with all theoretical developments, proving that the proposed power multiphase-multilevel conversion scheme is suitable to drive a dual three-phase induction motor with open-end stator winding configuration under healthy and post-fault conditions.

VI. REFERENCES

- [1] A.H. Bonnett, C. Yung, "Increased efficiency versus increased reliability," in *Conf. Proc. IEEE Ind. Appl. Mag.*, vol. 14, no. 1, Jan.–Feb. 2008.
- [2] A. Siddique, G. S. Yadava, B. Singh, "A review of stator fault monitoring techniques of induction motors," *IEEE Tran. on Ener. Conv.*, vol. 20, no. 1, March 2005.
- [3] A. Bellini, F. Filippetti, C. Tassoni, G. A. Capolino, "Advances in diagnostic techniques for induction machines," *IEEE Trans. on Ind. Electron.*, vol. 55, no. 12, Dec. 2008.
- [4] E. Levi, "Multiphase electric machines for variable-speed applications," *IEEE Trans. on Ind. Appl.*, vol. 55, no. 5, pp. 1893–1909, May 2008.
- [5] G. Grandi, G. Serra, A. Tani, "General analysis of multiphase systems based on space vector approach," in *Proc. Inter. Power Electron., and Motion Control Conf., EPE–PEMC'06*, Portoroz, Slovenia, pp. 834–840, 30 Aug.–1 Sep. 2006.
- [6] J. Rodriguez, S. Bernet, Bin Wu, J.O. Pontt, S. Kouro, "Multilevel voltage-source-converter topologies for industrial medium-voltage drives," *IEEE Trans. on Ind. Electron.*, vol. 54, no. 6, pp. 2930–2945, Dec. 2007.
- [7] L.G. Franquelo, J. Rodriguez, J.I. Leon, S. Kouro, R. Portillo, M. M. Prats, "The age of multilevel converters arrives," in *Proc. IEEE Ind. Electron., Magazine*, vol. 2, no. 2, pp. 28–39, June 2008.
- [8] S. Bolognani, M. Zordan, M. Zigliotto, "Experimental fault-tolerant control of a PMSM drive," *IEEE Trans. on Ind. Electron.*, vol. 47, no. 5, pp. 1134–1141, Oct. 2000.
- [9] R. L. de A. Ribeiro, C. B. Jacobina, E. R. C. da Silva, A. M. N. Lima, "Fault-tolerant voltage-fed PWM inverter ac motor drive systems," *IEEE Trans. on Ind. Electron.*, vol. 51, no. 2, pp. 439–446, Apr. 2004.
- [10] A.L. Julian, G. Oriti, "A comparison of redundant inverter topologies to improve voltage source inverter reliability," *IEEE Trans. on Ind. Appl.*, vol. 43, pp. 1371–1378, 2007.
- [11] S. Yang, A. Bryant, P. Mawby, D. Xiang, Li Ran, P. Tavner, "An industry-based survey of reliability in power electronic converters," *IEEE Trans. on Ind. Electron.*, vol. 47, no. 3, pp. 1441–1451, May–June 2011.
- [12] S. Yang, D. Xiang, A. Bryant, P. Mawby, Li Ran, P. Tavner, "Condition monitoring for device reliability in power electronic converters: A review," *IEEE Trans. on Power Electron.*, vol. 25, no. 11, pp. 2734–2752, Nov. 2010.
- [13] Y. Zhao, T.A. Lipo, "Space vector PWM control of dual three-phase induction machine using vector space decomposition," *IEEE Trans. on Ind. Appl.*, vol. 31, no. 5, pp. 1100–1109, Sept.–Oct. 1995.
- [14] G. Grandi, A. Tani, G. Serra, "Space vector modulation of six-phase VSI based on three-phase decomposition," in *Conf. Proc. IEEE 19th Symposium on Power Electron., Electrical Drives etc., SPEEDAM'08*, Taormina (IT), pp. 674–679, 11–13 June 2008.
- [15] Y. Kawabata, M. Nasu, T. Nomoto, E.C. Ejiogu, T. Kawabata, "High-efficiency and low acoustic noise drive system using open-winding AC motor and two space-vector-modulated inverters," *IEEE Trans. on Ind. Electron.*, vol. 49, no. 4, pp. 783–789, Aug. 2002.
- [16] J. Kim, J. Jung, K. Nam, "Dual-inverter control strategy for high-speed operation of EV induction motors," *IEEE Trans. on Ind. Electron.*, vol. 51, no. 2, pp. 312–320, Apr. 2004.
- [17] R. Kanchan, P. Tekwani, K. Gopakumar, "Three-level inverter scheme with common mode voltage elimination and dc link capacitor voltage balancing for an open-end winding induction motor drive," *IEEE Trans. on Power Electron.*, vol. 21, no. 6, pp. 1676–683, Nov. 2006.
- [18] G. Grandi, C. Rossi, A. Lega, D. Casadei, "Multilevel operation and input power balancing for a dual two-level inverter with insulated dc sources," *IEEE Trans. on Ind. Appl.*, vol. 44, no. 6, pp. 1815–1824, Nov.–Dec. 2008.
- [19] R. Bojoi, A. Tenconi, F. Farina, F. Profumo, "Dual-source fed multiphase induction motor drive for fuel cell vehicles: Topology and control," in *Proc. of 36th Power Electron., Specialists Conf., PESC'05*, Recife, Brazil, pp. 2676–2683, June 2005.
- [20] D.G. Holmes, T.A. Lipo, "Pulse width modulation for power converters: Principles and practice," *IEEE Press-John Wiley*, pp. 467–469, 2003.
- [21] G. Grandi, A. Tani, P. Sanjeevikumar, D. Ostojic, "Multi-phase multi-level ac motor drive based on four three-phase two-level inverters," in *Conf. Proc. IEEE 20th Symposium on Power Electron., Electrical Drives etc., SPEEDAM'10*, Pisa (IT), pp. 1768–1775, June 2010.
- [22] G. Grandi, Y. Gritli, F. Filippetti, C. Rossi, "Fault-tolerant operating analysis of a quad-inverter multiphase multilevel ac motor drive," in *Conf. Proc. IEEE-SDEMPED'11*, Bologna (IT), pp. 126–132, Sept. 2011.
- [23] G. Grandi, P. Sanjeevikumar, Y. Gritli, F. Filippetti, "Fault-tolerant control strategies for quad-inverter induction motor drives with one failed inverter," in *Proc. 20th Intl. Conf. on Electrical Machines, IECM'12*, Marseille (F), 2–5 Sept., 2012.
- [24] G. Grandi, D. Ostojic, "Dual inverter space vector modulation with power balancing capability," in *Proc. IEEE Region 8 Conf., EUROCON'09*, St. Petersburg (RUS), pp. 721–728, 18–23 May 2009.
- [25] G. Grandi, P. Sanjeevikumar, D. Casadei, "Preliminary hardware implementation of a six-phase quad-inverter induction motor drive," in *Proc. European Power Electron., and Appl., Conf., EPE'11*, Birmingham (UK), pp. 1–9, 30 Aug.–1 Sept. 2011.